Earth and Planetary Science Letters 534 (2020) 116070

Contents lists available at ScienceDirect

Earth and Planetary Science Letters

www.elsevier.com/locate/epsl

Reversible subsidence on the North West Shelf of Australia

Michael Gurnis [a,*], Michelle Kominz [b], Stephen J. Gallagher [c]

[a] Seismological Laboratory, California Institute of Technology, Pasadena, CA 91125, USA
[b] Department of Geological and Environmental Sciences, Western Michigan University, Kalamazoo, MI 49008, USA
[c] School of Earth Sciences, The University of Melbourne, Melbourne, VIC 3010, Australia

ARTICLE INFO

Article history:
Received 13 April 2019
Received in revised form 2 November 2019
Accepted 4 January 2020
Available online 17 January 2020
Editor: R. Bendick

Keywords:
tectonic subsidence
passive margins
dynamic topography plate flexure

ABSTRACT

The Northwest Shelf (NWS) of Australia is characterized by offshore basins associated with Permian and Jurassic rifting and was only slowly subsiding by the Neogene. International Ocean Discovery Program (IODP) Expedition 356 targeted this region by coring four sites in the Northern Carnarvon and Roebuck Basins and two sites in the Perth Basin to the south on the Australian western margin. We use detailed lithological, physical property and age data with paleobathymetric interpretations, to infer tectonic subsidence apparently confined to the NWS that reverses (uplifts) with about the same amplitude and rate as an earlier subsidence event. About 300 m of tectonic subsidence occurred over one million years from 6 to 5 million years ago and then reverses when 300 m of tectonic uplift occurred from 2 to 1 Ma. The along strike extent of this subsidence pattern is ~ 400 km. The similarity of magnitude and duration of the subsidence and uplift phases suggest that the subsidence is reversible. The results cannot be explained by glacial eustatic variability nor can the uplift event be attributed to sediments filling the accommodation space generated earlier. Reversible subsidence is a key fingerprint of dynamic topography. Although the rates of subsidence and uplift are roughly ~ 300 m/Myr, a substantial portion of the changes occur over less than 1 Myr and the rates inferred from a detailed least squares analysis can reach up to about 500 m/Myr. These rates are incompatible with dynamic topography associated with motion of Australia over large-scale convection (10 to 40 m/Myr) or that associated with instability of the base of the lithosphere (<15 m/Myr). The vertical motions are too large to be associated with simple flexure of a plate and plate buckling in that the required amplitudes would lead to permanent deformation of the plate. A new geodynamic mechanism is required to fit the observations.

1. Introduction

The Northwest Shelf (NWS) of Australia is a passive margin that developed since late Paleozoic time as micro-continents rifted from Australia when it was part of eastern Gondwana (Etheridge and O'Brian, 1994; Exon and Colwell, 1994; Hengesh et al., 2013; Longley et al., 2002). The latest phase of rifting occurred in the Late Jurassic (Exon and Colwell, 1994; Heine and Müller, 2005; Metcalfe, 1988) and since then the NWS has been relatively stable. However, since the breakup and dispersal of eastern Gondwana during the Cretaceous, Australia has moved several thousand kilometers northward, mostly since the Eocene, and has recorded anomalous marine inundation that cannot be reconciled with known global sea level variations (DiCaprio et al., 2009; Heine et al., 2010; Russell and Gurnis, 1994; Sandiford, 2007; Veevers, 2000). Interpreted shoreline positions suggest that the discrepancy is partly due to a long wavelength, downward tilting of Australia to the northeast by 300 m since the Eocene (DiCaprio et al., 2009). Backstripping of clinoform rollover positions indicates that margin-wide anomalous subsidence may have been broadly synchronous over the NWS and commenced at ~ 10 Ma with a down-to-the-north gradient (Czarnota et al., 2013). The amplitudes of inferred subsidence are broadly consistent with residual depth anomalies on adjacent oceanic crust (Czarnota et al., 2013).

Both residual depth anomalies (depth of the sea floor when normal thermal subsidence and isostatic effects of sediment loading and crustal thickness are removed) and the onshore and offshore vertical motions have been interpreted in terms of dynamic topography, the component of topography controlled by mantle convection and mantle mass anomalies. Three mechanisms have been proposed to explain the observed change in dynamic to-

* Corresponding author.
E-mail address: gurnis@gps.caltech.edu (M. Gurnis).

https://doi.org/10.1016/j.epsl.2020.116070
0012-821X/

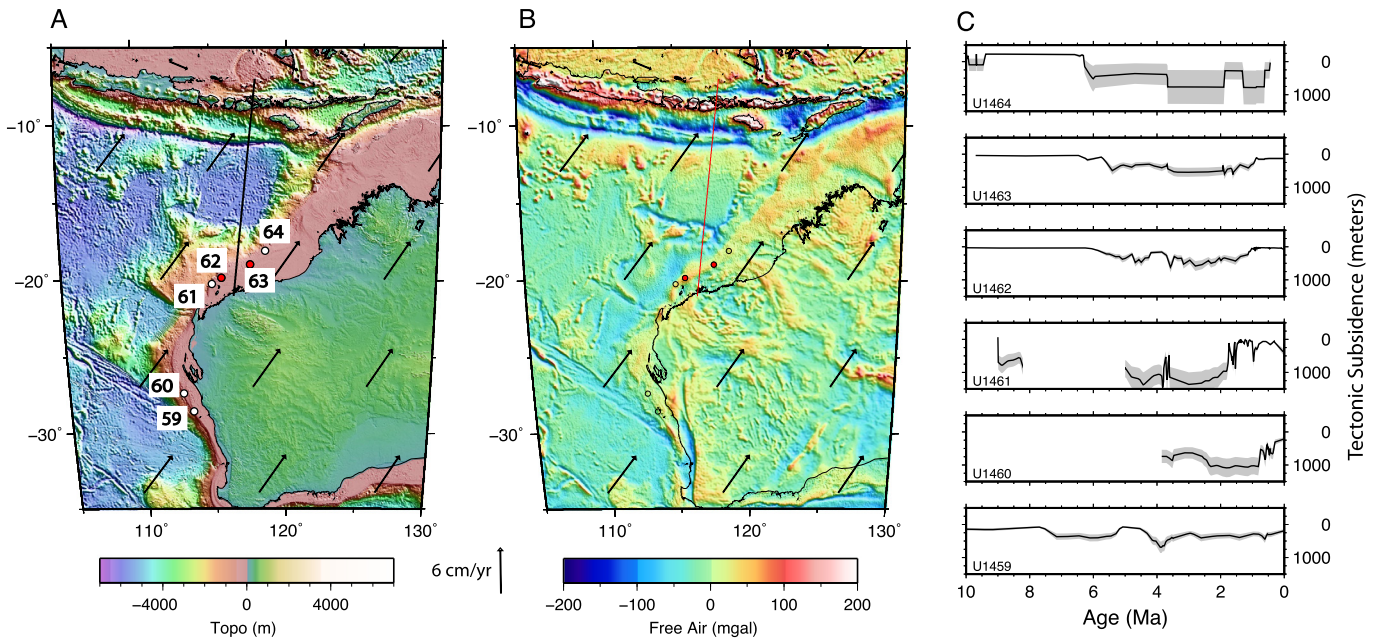

Fig. 1. A. Present day topography and B. free air gravity with location of IODP Sites shown with colored circles (those with red fill) are studied in detail. Overlain with present day plate motions with respect to hot-spots, with scale indicated below (Seton et al., 2012). In A, Sites are labeled as 59 for U1459, etc. C. Tectonic subsidence inferred for these sites; gray shading denotes uncertainty as region between minimum and maximum values. These tectonic subsidence curves, R1, have been shifted vertically so that they match the present water depths at these sites. (For interpretation of the colors in the figure(s), the reader is referred to the web version of this article.)

pography: the relatively fast vertical movement of mass anomalies within the mantle under slow-moving plates (Griffiths et al., 1989; Gurnis et al., 2000; Mitrovica et al., 1989), rapid motion of plates over slower moving mantle mass anomalies (Gurnis, 1990), and displacement of instabilities at the base of the lithosphere (Petersen et al., 2010). Given the long-wavelength pattern of a component of the signal, the Australian eustatic-discrepant vertical motions have been ascribed to long wavelength dynamic topography with motion of Australia towards downwelling slabs to the north of the continent and motion away from higher temperature mantle to the south of Australia during the Cenozoic (DiCaprio et al., 2011). Dynamic topography can produce vertical displacements over thousands of kilometers while lithospheric flexure produces vertical displacements over hundreds of kilometers (Gurnis, 1991; Mitrovica et al., 1989). Motion of the Australian plate toward either convective downwellings to the north or trench-induced flexure could be expected to produce a diachronous signal such that subsidence occurs earlier for northern points fixed to the plate. Alternatively, anomalous loads attached to the moving plate could produce synchronous vertical motions.

Although the Australian vertical motions have generally been interpreted within the context of large-scale dynamic topography, there continues to be debate on the length-scales, amplitudes and rates of change of dynamic topography. Globally, the analysis of residual topographies suggests that there are appreciable signals over length-scales ranging from 100's to 1,000's of km, which have been interpreted with mantle flow models (Davies et al., 2019; Hoggard et al., 2016; Yang et al., 2017). Dynamic topography changes as a function of time and constraints on vertical motions (mostly stratigraphic) have been interpreted within this context. The rates of change of long wavelength dynamic topography, from models and interpretation of observations, suggest rates that are generally <50 m/Myr (Gurnis et al., 2000). However, rates as high as 300 m/Myr, inferred from raised terraces on the west coast of Africa (Guiraud et al., 2010), have been interpreted in terms of convective uplift of the Angolan Dome (see discussion in Hoggard et al. (2016)).

We address the timing and amplitude of Miocene to recent vertical motions of the NWS recorded in cores recently recovered by International Ocean Discovery Program (IODP) Expedition 356, designed, in part, to better constrain the vertical motions of the NWS in time and space (Gallagher et al., 2017b). Here we present interpretations of detailed backstripping analysis of the six sites over a latitudinal range from 29° S to 18° S (Fig. 1A). We focus on the most northerly sites as these show an anomalous pattern of subsidence which is difficult to reconcile with existing scenarios of basin subsidence, dynamic topography or plate flexure. We attempt to characterize the vertical motion within the context of kinematic and dynamic models.

2. Subsidence analysis

The tectonic, or driving, subsidence was estimated using backstripping, an inverse approach using stratigraphic data (e.g., Watts and Ryan (1976)). We take a simple Airy (1-dimensional) approach to isostatic unloading, appropriate as the NWS maybe relatively weak lithosphere (McNutt and Parker, 1978). Our database consists of 6 drill sites spanning a distance of 1000 km, without the detailed two or three-dimensional data required for flexural modeling. We define tectonic subsidence (TS) as:

$$TS = S^* \left(\frac{\rho_a - \rho_{s*}}{\rho_a - \rho_w} \right) - \Delta SL \left(\frac{\rho_a}{\rho_a - \rho_w} \right) + WD \qquad (1)$$

where S* is decompacted sediment thickness, Δ SL the change in eustatic sea level and WD the paleoenvironment (water depth at any given time) at the drill site. Also ρ is the density of asthenosphere (subscript a), seawater (w) and decompacted sediment (s*). Rather than making an *a priori* assumption that we know what eustatic sea level change was, we consider the impact of eustasy in the discussion. Our estimate of tectonic subsidence without correcting for eustasy is R1 (Bond et al., 1989):

$$R1 = S^* \left(\frac{\rho_a - \rho_{s*}}{\rho_a - \rho_w} \right) + WD = TS + \Delta SL \left(\frac{\rho_a}{\rho_a - \rho_w} \right) \qquad (2)$$

Table 1
IODP 356 Sites used for analysis of tectonic subsidence.

Site	Lat	Long	Water depth (m)	Max penetration (mbsf)	Max age of recovered sediment (Ma)	Max apparent accumulation rate (cm/Kyr)	Adjacent industry well	Distance from IODP site (km)
U1459	28°40.26′ S	113°33.54′ E	192.3	400	48.31	15	Houtman-1	2
U1460	27°22.49′ S	112°55.43′ E	214.4	306.6	3.85	39	Morangie-1	0.125
U1461	20°12.85′ S	115°03.94′ E	127.5	1095.3	>5.59	52	West Tryal Rocks-2	0.125
U1462	19°49.28′ S	115°42.60′ E	87.2	950	5.59	70	Fisher-1	0.1
U1463	18°57.92′ S	117°37.43′ E	145.1	530	5.59	18	Picard-1	0.025
U1464	18°03.91′ S	118°37.89′ E	164.1	840	12.8	17		

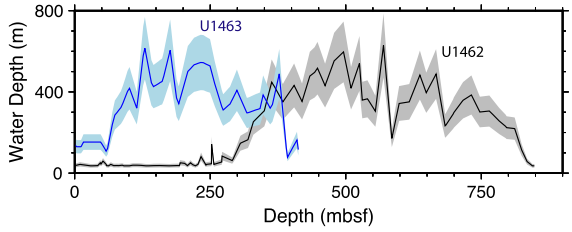

Fig. 2. Change in paleo water depth for Sites U1462 and U1463. See Fig. S1 for information on how the indicated error (shown with shaded) was computed.

Finally, when R1 is displayed, it will be referenced to present-day water depth at each site, and referred to as tectonic subsidence (Fig. 1C).

Expedition 356 recovered 28% to 97% of the sediment at the six sites. Depths of penetration range from 306 to 1095 mbsf (meters below sea floor) and maximum ages for each site range from 3.9 Ma to 48 Ma (Table 1). Most sites were triple cored and the sites were spliced for high resolution stratigraphic analysis (Gallagher et al. (2017a), Summary). The compaction of sediments below those cored by Expedition 356 is an important factor and constraints from nearby industry wells were placed beneath the IODP core-hole results (Table S1). There is no industry data available near Site U1464; consequently, 3000 m of mixed sediment was placed beneath that drill site. At Site U1462 (and the adjacent Fisher-1 industry well) new age and (paleo) water depth estimates were generated through interpretation of sediment and microfossil assemblages between 1221 and 964 mbsf.

The sediments recovered at the IODP sites are dominantly carbonates (mudstones, wackestones and packstones). They yielded excellent microfossils that provided excellent age control using planktonic foraminiferal and nannofossil datums calibrated to the Gradstein et al. (2012) biochronology (Gallagher et al., 2017b). Paleo-water depths were interpreted using benthic foraminiferal assemblages and ratios of planktonic to benthic foraminifera (using the method of Van der Zwaan et al. (1990) as modified by Van Hinsbergen et al. (2005)) in post-cruise analyses of Sites U1459, U1460, U1462 and U1463 (Buckley, 2016; Gallagher et al., 2017a,b). The error on the Van Hinsbergen et al. (2005) estimates is +/-20 m in similar Cenozoic strata on the southern margin of Australia (Gallagher et al., 2013). However, in this work we have used a more conservative error range described in the Supplementary Material (Fig. S1). These estimates were further corroborated by comparisons of core facies (Gallagher et al., 2018, 2014b) with modern carbonate facies in the region (Collins et al., 2014).

The paleo-depth estimates are summarized for Sites U1462 and U1463 (Fig. 2) where paleodepths are near modern conditions in the uppermost intervals. These facies are preceded by an interval of deep water biofacies that in turn overlies shallow water facies near the base of the cores. This type of integrated (bio)facies analysis was not performed on the strata from Site U1464 and the shipboard benthic and total foraminiferal assemblage data are here judged to be preliminary. The water depths for all other sites are shown in Figure S2. Although the uncertainty is large, initial subsidence at Site U1464 is consistent with the subsidence (timing and magnitude) at Sites U1462 and U1463. In addition, the upper section of U1464 has a high percentage of planktic foraminifera (>80%), which is interpreted as a localized deep water (>300 m paleodepths to present sea bed) plankton concentration due to the presence of a long lived plankton ridge (James et al., 2004). This limits paleobathymetric estimates for Site U1464 for the last several million years. At Site U1461, the lowermost section is characterized by a basal regional Miocene unconformity overlain by upper bathyal facies which continue until around 1.5 Ma (Gallagher et al., 2017b). Beneath the upper 500 m is a submarine slide (the Gorgon slide, Scarselli et al. (2013)) also limiting palaeobathymetric estimations. Nevertheless, the paleodepth change over the last several Myrs at Site U1461 is not inconsistent with the patterns at Sites U1462 and U1463. Finally, much further to the south in the Perth Basin, the paleo depth changes at Sites U1459 and U1460 are not consistent with one another: U1459 shows no substantial changes while U1460 shows an uplift similar to the NWS, but we have no constraint on any earlier subsidence. Thus, we exclude these southern wells from further analysis, but we do refer to these observations in our discussion of the length-scale of any vertical motion in the Discussion. Compaction of Neogene strata in each section was based on shipboard observations of porosity change with depth. Although variations in porosity are seen across the margin, no consistent lithology-based porosity versus depth trends were found in the IODP Exp. 356 data (Gallagher et al., 2017b). We used ship-based porosity versus depth curves for carbonates generated for each site. Older (Mesozoic to Cenozoic) sections in adjacent wells (calibrated from industry well completion data) added beneath the IODP sites were decompacted using the lithology-dependent porosity with depth relations of Kominz et al. (2011). Conservative paleodepth ranges (0-500 m) for older sequences in the adjacent wells beneath the cores at Sites U1462 and U1463 were inferred based on interpretations of facies and microfossils described in well completion reports (see Supplementary Material, Fig. S3). The age of these strata was estimated from biostratigraphic data in these reports and recalibrated to Gradstein et al. (2012).

The pre-Neogene tectonic subsidence curves generated from adjacent industry wells of the IODP Sites reflect the long-term subsidence of the NWS (Fig. S3), where episodes of rifting were followed by subsidence due to thermal cooling. The Morangie-1 well, in the northern Perth Basin shows the earliest subsidence which appears to date back to initial rifting of micro-fragments that are now part of the east Asian continent. Subsidence at the remainder of the well locations, including the southern Perth Basin (Houtman-1), and the Northern Carnarvon basin (West Tryal Rocks-2, Fisher-1 and Picard-1) show evidence of active rifting in the Triassic and Jurassic prior to rifting of additional terrains in the late Jurassic. Finally, there is some evidence of subsidence events within the 10 Myr period of time when India separated from western Australia in the middle of the Early Cretaceous. Subsidence in each of these locations appears to be fairly stable by the end of the

Paleogene, suggesting that this subsidence may have been dominated by thermal subsidence. However, during the middle of the Neogene there appears to have been a large tectonic event at all of these locations.

Northern Carnarvon and Roebuck Basins Sites U1461 to U1464 show evidence of rapid subsidence during the late Miocene (Fig. 1C). This event may have initiated at 9 Ma at Site U1461 (but is uncertain given missing record between 8 and 5 Ma), and about 6.2 Ma at Site U1462. This subsidence event ceases at Sites U1462 and U463 with a relatively rapid uplift event after 1.5 Ma We estimate the magnitude of uplift, from the maximum phase of subsidence (4 – 2 Ma) to the present to be about 300 m at Sites U1462 and U1463 (Fig. 1C). The limitations of the data at Sites U1459, U1460, U1461 and U1464 described above preclude them from the following subsidence analyses and modeling. We therefore interpret and analyze the subsidence histories at Sites U1462 and U1463 as these wells have the most robust data. These two wells show nearly identical timing and magnitudes of both subsidence and uplift (Fig. 1C).

3. Sensitivity

An unusual aspect of the vertical motions at Sites U1462 and U1463, is the apparent uplift between about 2 Ma and 1 Ma. Within the context of the magnitude of uplift required at Sites U1462 and U1463, we address the veracity of the signal and the possibility it could have arisen from glacio-eustatic change, uncertainties in analysis, or local factors.

Rapid shoaling can occur when sediments fill a basin. This may be particularly the case at the edge of a shelf where progradation may generate significant sediment thickness in a short period. The Airy unloading model accounts for this on a weak margin, such as the NWS. But if the margin has significant horizontal strength is considered with an infinitely rigid plate. In this case the bathymetric effect of addition of sediment is the change in total decompacted sediment thickness. That is, we are assuming that the added sediment compacts the underlying sediment but does not cause subsidence of the infinitely rigid lithosphere. The shoaling at Site U1463 occurred between 1.9 Ma and 0.8 Ma with a change in decompacted sediment thickness of 54 m. At Site U1462, while most of the uplift occurred in the same time frame, we maximize the effect of sediment addition on the uplift by considering the entire time period in which uplift occurred. This includes a 2 Myr period from 2.8 Ma to 0.8 Ma. Over that time interval, the decompacted sediment thickness increased from 3414 m to 3556 m, a change of 142 m. This means that the maximum amount of shoaling that could have resulted from sediment deposition is less than 142 m at Site U1462 and less than 54 m at Site U1463. We believe that this is a significant overestimate of the effect of adding sediment at the NWS. Never-the-less the uncertainties are less than the error estimates of water depth. As such the Airy-based tectonic subsidence (Fig. 1C) are entirely reasonable.

There is no indication that the rapid increase in depth observed at the NWS is an artefact of transport of benthic foraminifera to these sites from elsewhere. First, the stratigraphy from multichannel seismic data do not show any consistent tilting as would be expected from a prograding platform edge. Neogene strata at Sites U1462 (Fig. F3 in Gallagher et al. (2017c)) and U1463 (Fig. F3 in Gallagher et al. (2017d)) were deposited on a low angle ramp. If the benthic foraminifera were transported from elsewhere, presumably they would be shallow water species not deeper water ones in that sediment does not generally travel upslope. Finally, the age model at both sites is entirely progressive in time with no indication of intermixing (reworking) of planktonic foraminifera.

It is not possible to generate the observed variations in tectonic subsidence as a result of aliased sampling due to glacio-eustatic change. The magnitude of eustatic change inferred from proxies for changes in water mass (Lisiecki and Raymo, 2005) are small compared to the inferred NWS vertical motions. Water-mass changes provide the potential for sea-level variability with amplitudes of $\sim$ 100 meters occurring on timescales about 100 Kyr with a much smaller, long term trend since about 2.5 Ma of about 50 meters. These are all substantially smaller than the inferred $\sim$ 300 meter change at Sites U1462 and U1463.

Offshore mass-transport deposits caused by mass wasting are common along Australia's northwest margin and may have had an influence on vertical motions. The Gorgon Slide on the shelf edge west of Barrow Island is one of the largest submarine landslides identified in the region (McCormack and McClay, 2013), with a minimum estimated volume of 162 km^3 (Hengesh et al., 2013). Coring at IODP Site U1461 through this slide (Gallagher et al., 2017b) suggests it was triggered around 1 million years ago and its along strike length may be double previous estimates with a volume of $\sim$ 250 km^3. When added to previously mapped mass-transport deposits in the region the total volume amounts to at least $\sim$ 309 to 425 km^3 (Scarselli et al., 2013). Based on these observations we estimate the minimum cumulative volume displaced from the source at the continental rise to deeper waters was 309 km^3. Since these mass redistributions generally occur within the influence of plate flexure for Sites U1462 and U1463 we would expect that this would have influenced vertical motions at these drill sites.

If the mass was redistributed on an elastic plate, when material is removed from a slide-source area this would generally lead to uplift landward of the erosion event, impacting both the shelf and potentially the shoreline. The magnitude and sign of the vertical motions depend on the geometry and the mass of the slide, the relative position of the drill sites, and the nature of the elastic plate, estimated with a series of calculations. We have used two cumulative slide models, Model A and B (Table 2) in which the estimated volume of all of the slides is uniformly distributed across the area that they slid from. The sediment volume is subsequently uniformly distributed over the final location of the flows. Slide Model A approximately follows the areas of mapped slides on the Exmouth Plateau (Fig. S5, S6), but its cumulative volume is more than four times larger, 1,281 km^3, compared to the 309 km^3 estimated from seismic surveys and bathymetry (Hengesh et al., 2013). In addition, because the source area and the area of deposition of the slide are important factors, we have generated a volumetrically and spatially larger model, Model B, which both minimizes the distance between slides and drill sites and maximizes the area of the slide runoff (Fig. 3B). This model has a substantially over-estimated load, and consequently an over-estimate of the vertical motion induced by mass redistribution. If we assume that the source had a thickness of 100 meters (so that the volume is 1,713 km^3, 5.5 times larger than estimated seismically) both the uplift associated with mass removal (blue dashed, Fig. 3C) and the subsidence associated with placement of the mass load in the source area (blue dotted, Fig. 3C) are much smaller than those observed at the drill sites. The result is only a 14 meter change for an elastic plate with a rigidity, D, of 10^{20} N-m, not unreasonable for the Australian continent (McNutt and Parker, 1978). The vertical impact would be much smaller for plate rigidities typical of oceanic lithosphere. The loading problem is linear such that a factor of 5 increase in source thickness would lead to a commensurate increase in uplift at both sites. For the more realistic Slide A (Figure S5 and Table 2) the uplift at Site U1461 is 14 meters and at Site U1462 substantially smaller. By over-estimating all of the slide areas and thicknesses, optimally positioning the source and outflows of the slides, and minimizing the rigidity of the elastic plate, we obtain uplift estimates of several tens of meters (Fig. 3),

Table 2
Prediction for displacements for model landslides.

Slide	Source thickness (m)	Outflow thickness (m)	Vol (km^3)	Differential displacement at U1462 (m)	
				$D=10^{20}$ (N-m)	$D=10^{23}$ (N-m)
A	−500	122.17	1,281	14.24	0.37
B	−100	14.02	1,713	14.09	0.68

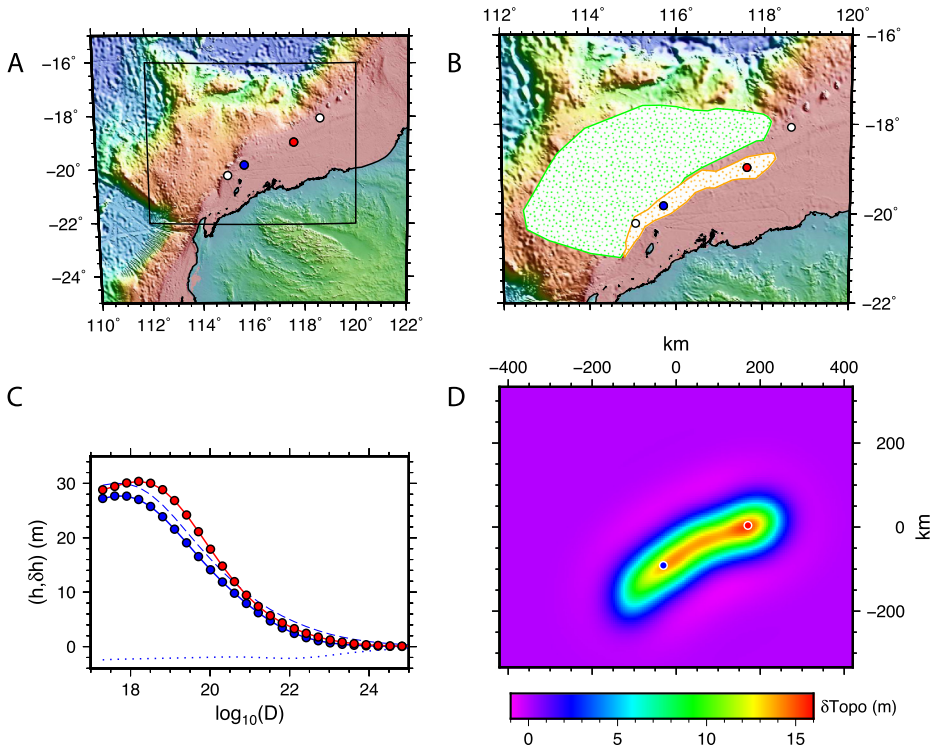

Fig. 3. Effect of mass wasting events on tectonic subsidence using slide Model B, which over-estimates cumulative slides inferred from seismic and drill hole data. A. Location of region of mass wasting model shown with black outline. B. Location of source (orange) and outflow (green) area of slide Model B with location of IODP Sites shown, including U1462 with filled blue circle and U1463 in red. C. Differential displacements at U1462 (filled blue circle) and U1463 (filled red circle) as a function of plate rigidity (with units N-m). Contributions from displacement associated with removal of mass at source and adding mass at the outflow for slide Model B at U1462 are shown with blue dashed and blue dotted lines, respectively. D. Differential vertical motion associated with moving a constant mass from the source to the sink on an elastic plate with a rigidity $D=10^{20}$ N-m computed onto a Cartesian domain (in km) with geographical locations mapped with equal area projection.

substantially smaller than the ∼ 300 meters of uplift required at Sites U1462 and U1463.

Since global sea level rise is much too small and the possible local mechanism of mass redistribution from mass wasting unable to provide sufficient uplift in the period between 2 and 1 Ma, it is likely that there must be an origin to the vertical motions that is deeper seated within the lithosphere or mantle.

4. Interpretive models

Tectonic subsidence over the NWS, especially at Sites U1462 and U1463, appears to have been roughly symmetrical in time and can be fit using least squares analysis by simple functions where the subsidence and uplift phases mirror one another (Fig. S4). Given the substantial uncertainties in tectonic subsidence, we have fit the Site U1462 and U1463 curves with the same function (a sinusoid for subsidence and uplift phases with constant values elsewhere) with amplitudes of 322 and 343 meters, giving maximum subsidence rates (or uplift rates) of 520 to 619 m/Myr (Fig. S4B).

Taking only rough estimates of the total tectonic subsidence, ∼ 300 meter, and the time period of subsidence, ∼ 1 Myr, gives ∼ 300 m/Myr, substantially smaller than the values recovered from the least squares analysis for the harmonic composite function (Fig. S4B). We have chosen this harmonic composite function because it provides an approximate fit to the data. Within uncertainty, the subsidence is reversed with subsequent uplift, perhaps with a smaller amount of remaining subsidence of 50 to 100 meters at Site U1463. There is clearly more signal than represented by these simple functions, but here we concentrate on the overall trend. Significantly, a key attribute of dynamic topography fixed to a mantle reference frame and sensed by a point fixed to a moving plate is a reversible signal (Gurnis et al., 1998), much like eustasy. This contrasts with most subsidence, i.e. permanent subsidence, characteristic of many sedimentary basin-forming mechanisms.

We investigate whether these amplitude and subsidence/uplift rates are consistent with a point fixed to a plate moving over a fixed pattern of dynamic topography with amplitudes and plate velocities bound realistic values. We assume that a point on the lithosphere moves with plate velocities of 0 to 25 cm/yr over a simple sinusoidal pattern of dynamic topography (with wavelengths from 100 to 2,000 km and amplitudes of 0 to 2 km). This results subsidence rates up to 10^3 m/Myr for plate velocities up to several 10's of cm/yr. When we compare these predicted rates in the domain of amplitude and velocity (Fig. 4C-E), they are not consistent with the inferred Site U1462 and U1463 tectonic subsi-

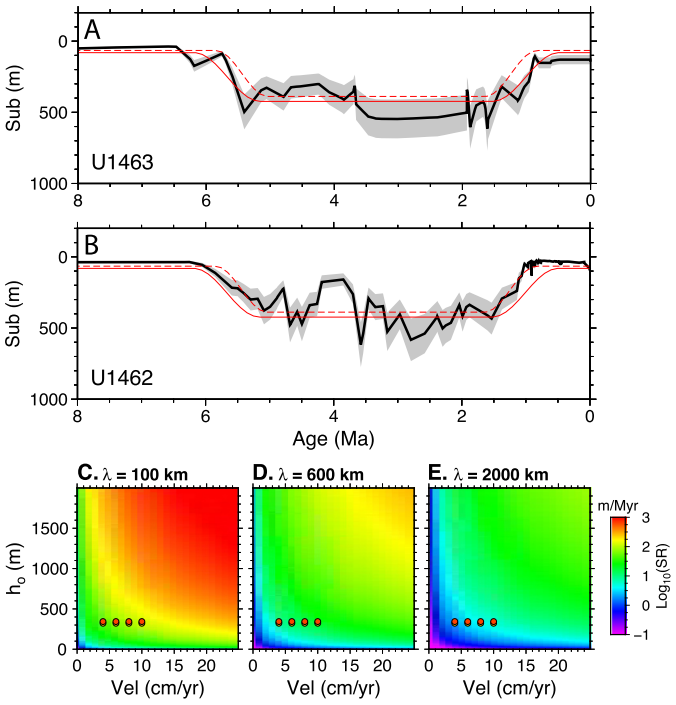

Fig. 4. Inferred tectonic subsidence (in black) shaded by maximum and minimum values compared against symmetrical function (discussed in text) for at Sites U1463 (A) and U1462 (B) with amplitudes 322 and 343 meters (dashed and solid red curves), the largest and smallest best fit amplitudes with respect to the background (see Fig. S4). Simple kinematic models for evolving topographies for three wavelengths 100 (C), 600 (D) and 2000 km (E) color corded by maximum subsidence rates (SR) in the domain of plate velocity (in cm/yr) versus amplitude of dynamic topography, h_o. Filled color circles are the rates of vertical motions inferred for sites U1462 and U1463 with reasonable plate tectonic velocities.

dence rates. The observed subsidence/uplift rates between $\sim$ 520 to 619 m/Myr (see Fig. S4B) exceed the predicted rates for any reasonable dynamic topography amplitude and wavelength and for any typical plate tectonic velocity for Australia. We will show that these combinations of amplitudes and wavelengths are not realistic in terms of the physics of mantle convection (see Supplementary Material and Section 4.2). Amplitudes of several km's at wavelengths of only a few 100 km are not expected and are only attained at the largest global scales (Gurnis et al., 2000; Hager and Richards, 1989). The subsidence rate has not been directly addressed for small-scale convection in the past (but addressed in Sec. 4.2).

The tectonic subsidence of the NWS is unusual and not consistent with pre-IODP Expedition 356 predictions (Gallagher et al., 2014a). Therefore, we explore a range of possible models to better understand the extent to which the data is consistent or inconsistent with geodynamic models, including, additional kinematic, mantle flow, lithospheric instability (small scale convection), flexural, and buckling models.

4.1. Kinematic models

Returning to kinematic models that now explicitly minimize their fit to observed tectonic subsidence curves, allows us to avoid the simple harmonic fits to the data used above. We use two approaches, passing the lithosphere over a fixed mantle anomaly and invoking a time-dependent lithospheric anomaly. With a set of forward models incorporating variable space and time patterns of dynamic topography we determine if it is possible to generate both the Site U1462 and U1463 tectonic subsidence curves. Although the kinematic models may fit the data, there is no guarantee that these patterns are realistic in terms of the physics of mantle flow (Supplementary Material) or small-scale convection (Section 4.2).

We move Australia with respect to a hotspot frame of reference (Seton et al., 2012) in which the hot-spots are essentially fixed since 11 Ma. The resulting NWS anomaly is a topographic depression, such that as the two IODP Sites move to the north over the anomaly they first subside and then uplift. A singular circular anomaly never fits both sites as anomalies with this functional form result in a diachronous subsidence and uplift. It is possible to obtain a better fit by assuming much more elongated anomalies. For example, by generating an anomaly defined by an ellipse smoothed in the easterly and northerly directions, but aligned NE to SW (Fig. S7), fits to the subsidence curves are possible including both the synchronicity between sites and an uplift phase that reverses the earlier subsidence. The example shown in Fig. S7 represents an elongated ellipsis and less elongated ones can fit the data equally well. The length-scale required for this model, defined in terms of an anomaly width, is on the order of 100 to 150 km. However, it is difficult to generate topographic anomalies like this with mantle flow generated by structures detached from the lithosphere (See Supplementary Material).

An alternative kinematic scenario is an anomaly that is fixed with respect to the lithosphere. In this case, the subsidence can be fit with a circular anomaly with a time-dependent amplitude that mirrors the observed subsidence and uplift (Fig. 5B). One can envision an axisymmetric convective instability at the base of the lithosphere that generates a smooth dynamic topography depression which we approximate as Gaussian in shape. The vertical motion of the earth's surface is driven by this Gaussian-shaped anomaly centered beneath the NWS at 3 Ma and with a fixed temporal variance of 1 Myr. The spatial variance and topographic amplitude are both variable with the best fit having an amplitude of 690 m and Gaussian width of 150 km (Fig. 5C). The maximum, instantaneous profile can be generated from a low temperature anomaly about 120 km across with a perturbation of 280° C (or 30 kg/m^3) fully embedded into the base of the lithosphere (Fig. 6B, S9). Although a circular spatial anomaly can fit the data well, models with long wavelengths, as evident from the minima in the L2 norm for any wavelength greater than about 100 km, can also fit the observed subsidence curves as long as the amplitude is around 600 meters (Fig. 5D). This suggests an insensitivity to the length-scale of the dynamic topography anomaly for these sites where there is no evidence of diachronous subsidence. Moreover, like the simple curve fit with a Gaussian (Fig. S4E-H), these models also suffer from underestimating the rates of subsidence and subsequent uplift phases (Fig. 5C) by about of factor of two.

4.2. Small-scale convection

Here we consider the possibility that small-scale convection within the mantle fits the patterns of subsidence and uplift with length-scales, amplitudes, and time-scales consistent with the observed tectonic subsidence curves. There has not been a systematic investigation of the rates of dynamic subsidence associated with small-scale convection, but because of the inherent reversibility of dynamic topography generated by convection, this model would seem to be a plausible explanation for the highly unusual NWS tectonic subsidence. Here we more fully explore this possibility with a series of two-dimensional computational models with different mantle viscosities and initial conditions (see Supplementary Material for computational details). The models have viscosities that are strongly dependent on temperature and stress, resulting in high frequency convective instabilities at the base of the lithosphere, as previously found, e.g., Huang et al. (2003). In another example, Petersen et al. (2010) suggested that these instabilities might explain small-amplitude, short duration sea-level variations.

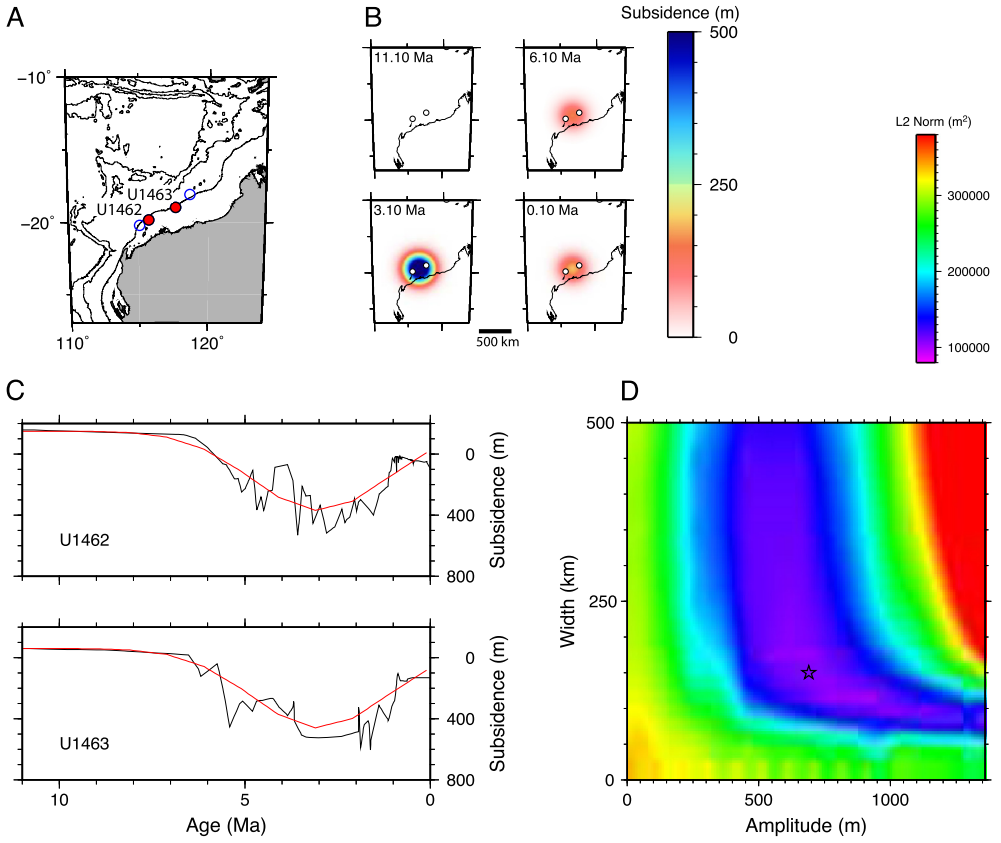

Fig. 5. A. Position of drill sites (blue open circles) including U1462 and U1463 (filled with red) used in the analysis. B-C. Best fitting kinematic model with a Gaussian circular subsidence pattern with a maximum amplitude of 690 m and a width of 150 km. In B is shown the changing vertical motion at 4 times in the past (11.1, 6.1, 3.1 0.1 Ma). C. Inferred tectonic subsidence (black lines) and best fitting model (red line). D. Misfit as an L2 norm for models with a range of amplitudes up to 1500 m and widths up to 500 km. Open black star denotes best fitting model.

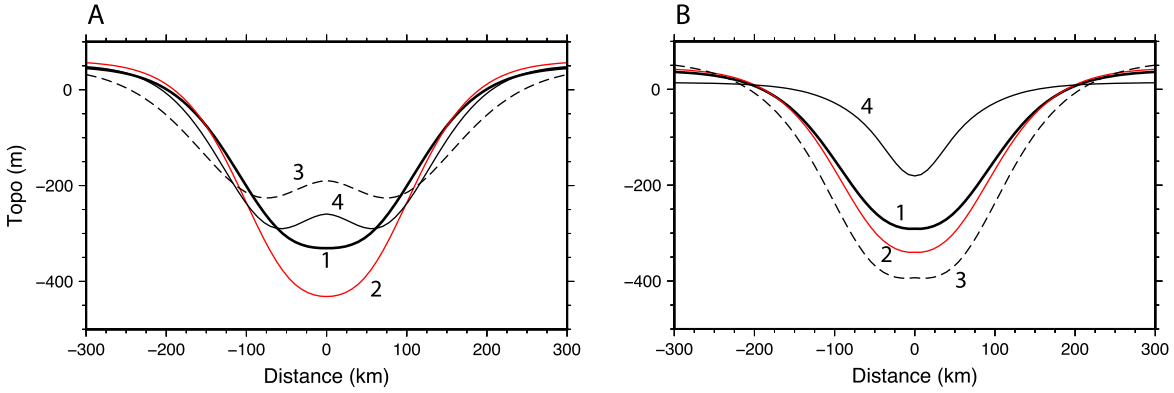

Fig. 6. Dynamic topographies predicted from flow models with assumed mantle anomalies (loads) that are either detached from the lithosphere (A) or attached to the lithosphere (B). Details on the models are provided in the Supplementary Material. In A, the lines are labeled 1-4 and refer to models Sink01-04, while in B the labels refer to models AL01-04. The profiles are centered on the middle of the mantle loads, exploiting the reflecting symmetry of the models shown in Fig. S8-S9.

Each model shows a transient phase dictated by initial conditions, which we exclude from the analysis. A typical model shows that there are Gaussian-like dynamic topography depressions associated with lithospheric anomalies with variances of ∼ 100 km (Fig. S10B). A spectral analysis of topography is used to find the highest amplitude signals from which we simultaneously extract the rate of change in topography. Subsidence rates varying up to about 15 m/Myr are associated with topographic amplitudes generally less than 100 meters at wavelengths between 100 and 1,000 km. Rates as high as 50 m/Myr are only found for a model with a longer wavelength of 1000 km (Fig. 7). The amplitudes are consistent with those in Petersen et al. (2010) but the rates of change are much smaller than those found at Sites U1462 and U1463.

4.3. Plate flexure

Subducting plates often display outer rises seaward of oceanic trenches (Watts, 2001; Watts and Talwani, 1974) with amplitudes of a few hundred meters and up to 500 meters in the case of the Mariana Trench (Turcotte, 1979). Outer rises are often attributed to flexure of an elastic plate (Turcotte, 1979), but flexure can also be generated by the high effective viscosity of the subducting oceanic plate (DeBremaecker, 1977; Zhong and Gurnis, 1994). There are

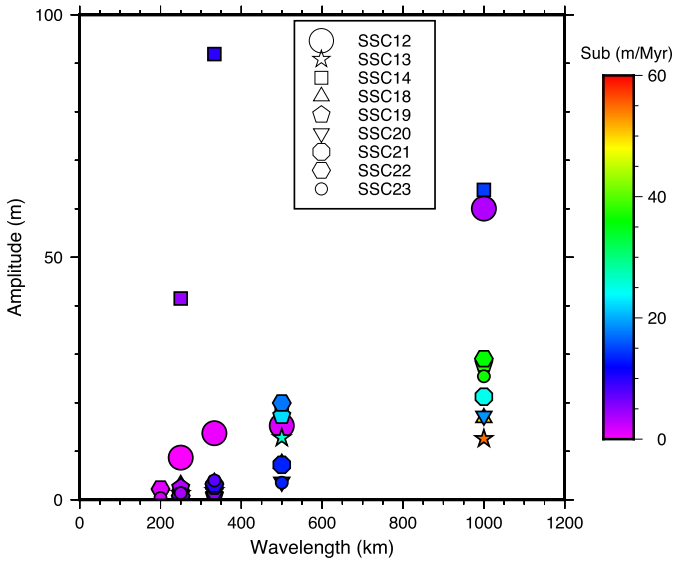

Fig. 7. Subsidence rate in the domain of the wavelength and amplitude of dynamic topography predicted in forward models of small-scale convection below the lithosphere. Each symbol represents a different model with either different mantle properties or initial conditions. Model numbers denoted in the legend are summarized in Table S3.

generally positive free-air gravity anomalies associated with the outer rise (Watts and Talwani, 1974) as can be seen for the Timor Trench, which the Australian Plate is moving toward (Fig. 1B). As a subducting plate moves toward the trench, a point fixed to the plate will tend to uplift (as it moves through the outer rise) and then subside as it enters the oceanic trench. Such signals have been used in the interpretation of the geology of islands moving toward oceanic trenches, such as for Niue in the Cook Islands about 270 km from and moving toward the Tonga Trench (Dubois et al., 1975). This island experienced about 70 meters of uplift as is evident from the elevation above sea level of the former atoll. To the northwest of the NWS, Christmas Island is about 100 km from the Java Trench, in the current position of the outer rise and has experienced about 100 meters of uplift (Woodroffe, 1988).

The current positions of Sites U1462 and U1463 are about 500 km from the present axis of the outer rise of the Timor Trench (Figure S11D). By fitting topographic profiles to the bathymetry around the Timor Trench, we are able to obtain a good fit with an elastic plate (using the universal solution of the deflection of an elastic plate (Turcotte, 1979)), however, there is only a small (less than one meter) deflection near the drill sites (Figure S11D). There would have been even smaller signals in the past when the vertical motions of the NWS occurred. Consequently, we can rule out the influence of vertical forces at the edge of the Australian Plate as being the cause of the apparent reversal in subsidence.

5. Discussion and conclusions

With detailed observations (lithology, physical properties, depositional ages and paleobathymetry) from IODP coring sites on the western margin of Australia, we have inferred a highly unusual pattern of tectonic subsidence that reverses (uplifts) with about the same amplitude and rate as the earlier subsidence. We call this reversible subsidence. The overall characteristics of the event is about a 300 m tectonic subsidence event that occurred over one million years from 5 to 6 million years ago. There was no systematically consistent vertical motion between the sites over the following three million years from 5 to 2 Ma. But from 2 to 1 Ma there was a 300 m tectonic uplift event that occurred over about one million years. The pattern between the two IODP Sites U1462 and U1463 are remarkably similar despite the fact that the thickness of the sediments has about a factor of two difference between them (Fig. 2); the events occur over about 800 meters at Site U1462 and about 400 meters at Site U1463. The depositional characteristics at the two nearby Sites U1461 and U1464 are less well determined, but the inferred tectonic subsidences at these two sites are not inconsistent with the clear reversible subsidence pattern inferred at Sites U1462 and U1463. Together, the distances spanned by these two sites is 400 km. There is no evidence from the two IODP Sites much further to the south, Sites U1459 and U1460, that they experienced such rapid and usual tectonic subsidence and uplift.

The vertical motions seem to be confined to the continental shelf. If the subsidence at around 4 Ma was of much longer wavelength and not confined to the shelf and with an amplitude of 200 m, then inundation would extend to about 100 km onshore (Fig. S12). If the amplitude was 400 meters, then the inundation could extend substantially further, such that nearly all of Western Australia would experience marine inundation (Fig, S12). However, the shoreline in the late Neogene, was not much different than it is today. In other words, there are no regionally significant late Neogene marine sediments (Langford et al., 1995). Consequently, the vertical motions were apparently confined to the offshore regions of north western Australia, but if these motions were confined to just the shelf or not remains unclear. Unfortunately, we are unable to constrain the amplitudes of vertical motions ($\sim$ 500 meters) of the oceanic crust seaward of the IODP Sites given the much greater water depths there.

These changes in tectonic subsidence are much larger in amplitude than late Neogene changes in sea level, associated with changing volumes of ice caps inferred from changes in the isotopic composition of the oceans (Lisiecki and Raymo, 2005; Miller et al., 2005). Although mass wasting from large debris flows is an important feature of the NWS, even when we over-estimate the volumes of mass redistribution by a factor of five, we still only predict vertical motions of 10's of meters not the 300 meters associated with the reversible subsidence.

IODP Expedition 356 was partly motivated to test a Cenozoic dynamic topography-induced subsidence of the NWS. Conceptually, the diagnostic manifestation of dynamic topography is an entirely reversible signal, that is a tectonic subsidence followed by uplift with about the same amplitude and time-scale (Gurnis et al., 1998). However, the amplitude and time-scale inferred for the NWS are much too rapid (potentially more than 500 m/Myr) to be consistent with rapidly changing small-amplitude vertical motions induced by lithospheric instabilities ($<$15 m/Myr) or from slower changing high amplitude anomalies induced by the northward motion of Australia (1-50 m/Myr). Shephard et al. (2010) discuss the rates of change of dynamic topography at large-scales associated with the motion of a continent over a slab in which she finds rates of 10 to 40 m/Myr. The alternative, key constraint on small-scale convection below the NWS would be seismic images. Seismic images of the Australian lithosphere and upper mantle reveal high compressional velocities (potentially associated with lower temperatures associated with convection) associated with the cratonic portion of the plate down to depths of 200-400 km (Fichtner et al., 2009). The mantle or lithosphere anomalies that could be responsible for the NWS subsidence could have thermal anomalies amounting to about 25% of the temperature drop across the lithosphere, $\sim$ 350° C; these could be associated with shear wave perturbations amounting to $\sim$ 1-2% of background values using derivatives of elastic properties with respect to temperature (Oganov et al., 2001). However, the putative structures have length-scales of $\sim$ 100 km across which are below the resolution of the seismic tomographic inversions available in this region, currently only about 500 km in scale (Fichtner et al., 2009). Explicit

tests with seismic results will require higher resolution local seismic surveys.

From the new, high frequency and NWS-isolated vertical motions, there is not necessarily any reason to refute the large-scale and longer term estimates of Australian tectonic motion, as either inferred from paleo-shorelines (DiCaprio et al., 2009; Sandiford, 2007) or from backstripping of clinoform rollover positions (Czarnota et al., 2013). We do note that there is potentially about 100 meters of cumulative subsidence at Site U1463 from about 7 to 6 Ma to about 1 Ma. This gives a rate of subsidence about 20 m/Myr which is consistent with the rates inferred earlier for the long term subsidence of the northern parts of Australia and from models of changing dynamic topography at long wavelengths (DiCaprio et al., 2011). It seems quite reasonable to hypothesize that there are two mechanisms of vertical motion: A slower, progressive long-wavelength component and a higher frequency and NWS-localized reversible component. The origin of the higher frequency component remains unknown.

A possibility for the rapid reversible subsidence could be linked to in-plane stresses associated with interaction of the subducting Australian plate with the Timor Trench. Simple plate flexure, explored above, is incapable of giving rise to the magnitude of deflections inferred on the NWS. Alternatively, in-plane stresses can act over much longer wavelengths (Cloetingh, 1988). Such intraplate stresses have been suggested to cause perturbations in basin subsidence on the order of 10's of meters (Cloetingh et al., 1985). The perturbations arise in those locations with significant vertical loads on an otherwise homogeneous elastic plates but amplitudes as large as 300 meters have not been found in such models. Alternatively, if the plate was placed in a large enough state of compression, then it could buckle, and the resulting folds could have amplitudes of the required magnitude. Indeed, the folds found within the Indian oceanic plate to the west of the NWS occur over a scale of 100-300 km with amplitudes of 1 to 3 km (Weissel et al., 1980). The timing for compressive stresses within the region of the NWS could have been driven by the collision of the Australian continental lithosphere with the Timor Trench. At 6 Ma the most distal parts of the Australian basement started to underthrust the deep accretionary ridge of the Banda Arc (Harris, 2011). Several parts of Australia have been subjected to Neogene tectonic activity including both the NWS (Keep et al. (2018) and references therein) and SE Australia (Dickinson et al., 2001, 2002).

Nevertheless, a traditional buckling model is problematic. There is no evidence of folding with the required amplitude and wavelength in the sediments of the NWS. Buckling could generate uplift and subsidence of the required amplitude, but why would subsidence reverse? When high amplitude buckling of plates is observed, deformation of the crust is permanent, as apparently occurred within the Indian plate itself (Weissel et al., 1980).

Interestingly, the mass wasting events which occurred over the NWS in the last 1 million years, may be a consequence of reversed subsidence. Conceptually, the rapid shallowing (uplift of the basement) essentially pushes unconsolidated carbonate muds upward, decompressing and weakening the strata and creating greater relief on the continental slope. This could have caused the mud-rich strata to destabilize on a regional scale triggering mass transport events. Major changes in eustatic sea level in the mid Pleistocene could have also enhanced and triggered this slumping process, especially as several high amplitude (+/-100 m) glacio-eustatic sea level changes occurred during the time of uplift.

We are unable to provide a satisfactory explanation for this unusual subsidence/uplift behavior described above. Normal tectonic processes apparently do not fit the observations. Consequently, the fundamental challenge is to advance a new hypothesis. The following characteristics seem to be required: Reversible subsidence occurring over at least 400 km along the strike of a passive margin with an amplitude of about 300 meters on time-scales of about one million years. The vertical motions were confined to the passive margin and could have been induced by compressional stresses through interaction of the continental lithosphere with the oceanic trench while avoiding buckling with permanent lithospheric deformation.

Declaration of competing interest

The authors declare that they have no known competing financial interests or personal relationships that could have appeared to influence the work reported in this paper.

Acknowledgements

USSSP supported the participation of MG and MK on IODP Expedition 356 as well as with post expedition awards. MG was also supported by the NSF through EAR-1645775. Funding to SJG was provided by the Australian IODP office and the ARC Basins Genesis Hub (IH130200012).

Appendix A. Supplementary material

Supplementary material related to this article can be found online at https://doi.org/10.1016/j.epsl.2020.116070.

References

Bond, G.C., Kominz, M.A., Steckler, M.S., Grotzinger, J.P., 1989. Role of thermal subsidence, flexure and eustasy in the evolution of early Paleozoic passive-margin carbonate platforms. In: Crevello, P.D., Wilson, J.L., Sarg, J.F., Read, J.F. (Eds.), Controls on Carbonate Platform and Basin Development, pp. 39–61. Specl. Publ. SEPM (Soc. Sediment. Geol.).

Buckley, T., 2016. Cenozoic Stratigraphy of the North Perth Basin and the Formation of the Houtman Abrolhos. University of Melbourne, Melbourne, Australia, p. 190.

Cloetingh, S., 1988. Intraplate stresses: a new element in basin analysis. In: Kleinspehn, K.L., Paola, C. (Eds.), New Perspectives in Basin Analysis. Springer, New York, NY, pp. 205–230.

Cloetingh, S., McQueen, H., Lambeck, K., 1985. On a tectonic mechanism for regional sealevel variations. Earth Planet. Sci. Lett. 15, 157–166.

Collins, L.B., James, N.P., Bone, Y., 2014. Carbonate shelf sediments of the western continental margin of Australia. Mem. Geol. Soc. Lond. 41, 255–272.

Czarnota, K., Hoggard, M.J., White, N., Winterbourne, J., 2013. Spatial and temporal patterns of Cenozoic dynamic topography around Australia. Geochem. Geophys. Geosyst. 14, 634–658.

Davies, D.R., Valentine, A.P., Kramer, S.C., Rawlinson, N., Hoggard, M.J., Eakin, C.M., Wilson, C.R., 2019. Earth's multi-scale topographic response to global mantle flow. Nat. Geosci. 12, 845–850.

DeBremaecker, J.-C., 1977. Is the oceanic lithosphere elastic or viscous? J. Geophys. Res. 82, 2001–2004.

DiCaprio, L., Gurnis, M., Müller, R.D., 2009. Long-wavelength tilting of the Australian continent since the Late Cretaceous. Earth Planet. Sci. Lett. 278, 175–185.

DiCaprio, L., Gurnis, M., Müller, R.D., Tan, E., 2011. Mantle dynamics of continent-wide Cenozoic subsidence and tilting of Australia. Lithosphere 3, 311–316.

Dickinson, J.A., Wallace, M.W., Holdgate, G.R., Daniels, J., Gallagher, S.J., Thomas, L., 2001. Neogene tectonics in SE Australia: implications for petroleum systems. APPEA J., 37–52.

Dickinson, J.A., Wallace, M.W., Holdgate, G.R., Gallagher, S.J., Thomas, L., 2002. Origin and timing of the Miocene-Pliocene unconformity in Southeast Australia. J. Sediment. Res. 72, 288–303.

Dubois, J., Launay, J., Recy, J., 1975. Some new evidence on lithospheric bulges close to island arcs. Tectonophysics 26, 189–196.

Etheridge, M.A., O'Brian, G.W., 1994. Structural and tectonic evolution of the Western Australian margin basin system. Pet. Explor. Soc. Aust. J. 22, 45–63.

Exon, N.F., Colwell, J.B., 1994. Geological history of the outer North West Shelf of Australia: a synthesis. AGSO J. Aust. Geol. Geophys. 15, 177–190.

Fichtner, A., Kennett, B.L.N., Igel, H., Bunge, H.-P., 2009. Full seismic waveform tomography for upper-mantle structure in the Australasian region using adjoint methods. Geophys. J. Int. 179, 1703–1725.

Gallagher, S.J., Fulthorpe, C.S., Bogus, K., Auer, G., Baranwal, S., Castañeda, I.S., Christensen, B.A., De Vleeschouwer, D., Franco, D.R., Groeneveld, J., Gurnis, M., Haller, C., He, Y., Henderiks, J., Himmler, T., Ishiwa, T., Iwatani, H., Jatiningrum, R.S., Kominz, M.A., Korpanty, C.A., Lee, E.Y., Levin, E., Mamo, B.L., McGregor, H.V., McHugh, C.M., Petrick, B.F., Potts, D.C., Rastegar Lari, A., Renema, W., Reuning, L., Takayanagi, H., Zhang, W., 2017a. Expedition 356: Indonesian Throughflow. In: Proceedings of the International Ocean Discovery Program, pp. 1–372.

Gallagher, S.J., Fulthorpe, C.S., Bogus, K., Auer, G., Baranwal, S., Castañeda, I.S., Christensen, B.A., De Vleeschouwer, D., Franco, D.R., Groeneveld, J., Gurnis, M., Haller, C., He, Y., Henderiks, J., Himmler, T., Ishiwa, T., Iwatani, H., Jatiningrum, R.S., Kominz, M.A., Korpanty, C.A., Lee, E.Y., Levin, E., Mamo, B.L., McGregor, H.V., McHugh, C.M., Petrick, B.F., Potts, D.C., Rastegar Lari, A., Renema, W., Reuning, L., Takayanagi, H., Zhang, W., 2017b. In: Proceedings of the International Ocean Discovery Program, Expedition 356: Indonesian Throughflow.

Gallagher, S.J., Fulthorpe, C.S., Bogus, K., Auer, G., Baranwal, S., Castañeda, I.S., Christensen, B.A., De Vleeschouwer, D., Franco, D.R., Groeneveld, J., Gurnis, M., Haller, C., He, Y., Henderiks, J., Himmler, T., Ishiwa, T., Iwatani, H., Jatiningrum, R.S., Kominz, M.A., Korpanty, C.A., Lee, E.Y., Levin, E., Mamo, B.L., McGregor, H.V., McHugh, C.M., Petrick, B.F., Potts, D.C., Rastegar Lari, A., Renema, W., Reuning, L., Takayanagi, H., Zhang, W., 2017c. Site U1462. In: Gallagher, S.J., Fulthorpe, C.S., Bogus, K., the Expedition 356 Scientists (Eds.), Proceedings of the International Ocean Discovery Program.

Gallagher, S.J., Fulthorpe, C.S., Bogus, K., Auer, G., Baranwal, S., Castañeda, I.S., Christensen, B.A., De Vleeschouwer, D., Franco, D.R., Groeneveld, J., Gurnis, M., Haller, C., He, Y., Henderiks, J., Himmler, T., Ishiwa, T., Iwatani, H., Jatiningrum, R.S., Kominz, M.A., Korpanty, C.A., Lee, E.Y., Levin, E., Mamo, B.L., McGregor, H.V., McHugh, C.M., Petrick, B.F., Potts, D.C., Rastegar Lari, A., Renema, W., Reuning, L., Takayanagi, H., Zhang, W., 2017d. Site U1463. In: Gallagher, S.J., Fulthorpe, C.S., Bogus, K., the Expedition 356 Scientists (Eds.), Proceedings of the International Ocean Discovery Program.

Gallagher, S.J., Fulthorpe, C.S., Bogus, K.A., 2014a. Reefs, oceans, and climate: a 5 million year history of the Indonesian Throughflow, Australian monsoon, and subsidence on the Northwest Shelf of Australia. In: International Ocean Discovery Program Scientific Prospectus 356.

Gallagher, S.J., Reuning, L., Himmler, T., Henderiks, J., De Vleeschouwer, D., Groeneveld, J., Rastigar, A., Fulthorpe, C.S., Bogus, K., Scientists, E.S., 2018. The enigma of rare Quaternary oolites in the Indian and Pacific Oceans: a result of global oceanographic physicochemical conditions or a sampling bias. Quat. Sci. Rev. 200, 114–122.

Gallagher, S.J., Villa, G., Drysdale, R.N., Wade, B.S., Scher, H., Li, Q., Wallace, M.W., Holdgate, G.R., 2013. A near field sea level record of East Antarctic Ice Sheet instability from 32 to 27 million years ago. Paleoceanography 28, 1–13.

Gallagher, S.J., Wallace, M.W., Hoiles, P.W., Southwood, J.M., 2014b. Seismic and stratigraphic evidence for reef expansion and onset of aridity on the Northwest Shelf of Australia during the Pleistocene. Mar. Pet. Geol. 57, 470–481.

Gradstein, F.M., Ogg, J.G., Schmitz, M.D., Ogg, G.M., 2012. The Geologic Time Scale of 2012. Elsevier.

Griffiths, R.W., Gurnis, M., Eitelberg, G., 1989. Holographic measurements of surface topography in laboratory models of mantle hotspots. Geophys. J. 96, 477–495.

Guiraud, M., Buta-Neto, A., Quesne, D., 2010. Segmentation and differential post-rift uplift at the Angola margin as recorded by the transform-rifted Benguela and oblique-to-orthogonal-rifted Kwanza basins. Mar. Pet. Geol. 27, 1040–1068.

Gurnis, M., 1990. Bounds on global dynamic topography from Phanerozoic flooding of continental platforms. Nature 344, 754–756.

Gurnis, M., 1991. Continental flooding and mantle-lithosphere dynamics. In: Sabadini, R., Lambeck, K., Boschi, E. (Eds.), Glacial Isostasy, Sea-Level, and Mantle Rheology. Kluwer Academic Publishers, Dordrect, pp. 445–492.

Gurnis, M., Mitrovica, J.M., Ritsema, J., van Heijst, H.-J., 2000. Constraining mantle density structure using geological evidence of surface uplift rates: the case of the African superplume. Geochem. Geophys. Geosyst. 1, 1–35.

Gurnis, M., Müller, R.D., Moresi, L., 1998. Dynamics of Cretaceous vertical motion of Australia and the Australian-Antarctic discordance. Science 279, 1499–1504.

Hager, B.H., Richards, M.A., 1989. Long-wavelength variations in Earth's geoid: physical models and dynamical implications. Philos. Trans. R. Soc. Lond. A 328, 309–327.

Harris, R., 2011. The nature of the Banda arc–continent collision in the Timor region. In: Brown, D., Ryan, P.D. (Eds.), Arc Continent Collision, Frontiers in Earth Sciences. Springer Verlag, Berlin, Germany, pp. 163–211.

Heine, C., Müller, R.D., 2005. Late Jurassic rifting along the Australian North West Shelf: margin geometry and spreading ridge configuration. Aust. J. Earth Sci. 52, 27–39.

Heine, C., Müller, R.D., Steinberger, B., DiCaprio, L., 2010. Integrating deep Earth dynamics in paleogeographic reconstructions of Australia. Tectonophysics 483, 135–150.

Hengesh, J.V., Dirstein, J.K., Stanley, A.J., 2013. Landsclide geomorphology along the Exmouth Plateau continental margin, North West Shelf, Australia. Aust. Geomech. J., Spec. Offshore Ed., 71–92.

Hoggard, M., White, N., Al-Attar, D., 2016. Global dynamic topography observations reveal limited influence of large-scale mantle flow. Nat. Geosci. 9.

Huang, J., Zhong, S., van Hunen, J., 2003. Controls on sublithospheric small-scale convection. J. Geophys. Res. 108.

James, N.P., Bone, Y., Kyser, T.K., Dix, G.R., Collins, L.B., 2004. The importance of changing oceanography in controlling late Quaternary carbonate sedimentation on a high energy, tropical, oceanic ramp: north-western Australia. Sedimentology 51, 1–27.

Keep, M., Holbourn, A., Kunht, W., Gallagher, S.J., 2018. Progressive Western Australian collision with Asia: implications for regional orogography, oceanography, climate and marine biota. J. R. Soc. West. Aust. 101, 1–17.

Kominz, M.A., Patterson, K., Odette, D., 2011. Lithology dependence of porosity in slope and deep marine sediments. J. Sediment. Res. 81, 730–742.

Langford, R.P., Wilford, G.E., Truswell, E.M., Isern, A.R., 1995. Palaeogeographic Atlas of Australia – Cainozoic, Cretaceous, vol. 10. Australian Geological Survey Organisation, Canberra, ACT, Australia.

Lisiecki, L.E., Raymo, M.E., 2005. A Pliocene-Pleistocene stack of 57 globally distributed d18 O records. Paleoceanography 20.

Longley, I.M., Buessenschuett, C., Clydsdale, L., Cubitt, C.J., Davis, R.C., Johnson, M.K., Marshall, N.M., Murray, A.P., Somerville, R., Spry, T.B., Thompson, N.B., 2002. The north west shelf of Australia—a Woodside perspective. In: Keep, M., Moss, S.J. (Eds.), The Sedimentary Basins of Western Australia. Petroleum Exploration Society of Australia, Perth, Australia, pp. 27–88.

McCormack, K.D., McClay, K., 2013. Structural architecture of the Gorgon Platform, North West Shelf, Australia. In: West Australian Basins Symposium. Perth, WA, Australia, pp. 1–23.

McNutt, M.K., Parker, R.L., 1978. Isostasy in Australia and the evolution of the compensation mechanism. Science 199, 1773–1775.

Metcalfe, I., 1988. Origin and assembly of south-east Asian continental terranes. In: Audley-Charles, M.G., Hallam, A. (Eds.), Gondwana and Tethys. Geological Society Special Publication, pp. 101–118.

Miller, K.G., Kominz, M.A., Browning, J.V., Wright, J.D., Mountain, G.S., Katz, M.E., Sugarman, P.J., Cramer, B.S., Christie-Blick, N., Pekar, S.F., 2005. The Phanerozoic record of global sea-level change. Science 310, 1293–1298.

Mitrovica, J.X., Beaumont, C., Jarvis, G.T., 1989. Tilting of continental interiors by the dynamical effects of subduction. Tectonics 8, 1079–1094.

Oganov, A.R., Brodholt, J.P., Price, J.D., 2001. The elastic constants of MgSiO3 perovskite at pressures and temperatures of the Earth's mantle. Nature 411, 934–937.

Petersen, K.D., Nielsen, S.B., Clausen, O.R., Stephenson, R., Gerya, T., 2010. Small-scale mantle convection produces stratigraphic sequences in sedimentary basins. Science 329, 827–830.

Russell, M., Gurnis, M., 1994. The planform of epeirogeny: vertical motions of Australia during the Cretaceous. Basin Res. 6, 63–76.

Sandiford, M., 2007. The tilting continent: a new constraint on the dynamic topographic field from Australia. Earth Planet. Sci. Lett. 261, 152–163.

Scarselli, N., McClay, K., Elders, C., 2013. Submarine slide and slump complexes, Exmouth Plateau, NW Shelf of Australia. In: Keep, M., Moss, S.J. (Eds.), The Sedimentary Basins of Western Australia 3. In: Proceedings of the Petroleum Exploration Society of Australia, Perth, WA, Australia.

Seton, M., Müller, R.D., Zahirovic, S., Gaina, C., Torsvik, T., Shephard, G., Talsma, A., Gurnis, M., Turner, M., Maus, S., Chandler, M., 2012. Global continental and ocean basin reconstructions since 200 Ma. Earth-Sci. Rev. 113, 212–270.

Shephard, G.E., Müller, R.D., Liu, L., Gurnis, M., 2010. Miocene Amazon River drainage reversal driven by plate-mantle dynamics. Nat. Geosci. 3, 870–875.

Turcotte, D.L., 1979. Flexure. Adv. Geophys. 21, 51–86.

Van der Zwaan, G.J., Jorissen, F.J., de Stigter, H.C., 1990. The depth dependency of planktic/benthic foraminiferal ratios: constraints and applications. Mar. Geol. 95, 1–16.

Van Hinsbergen, D.J.J., Kouwenhoven, T.J., van der Zwaan, G.J., 2005. Paleobathymetry in the backstripping procedure: correction for oxygenation effects on depth estimates. Palaeogeogr. Palaeoclimatol. Palaeoecol. 221, 245–265.

Veevers, J.J., 2000. Billion-Year Earth History of Australia and Neighbours in Gondwanaland. Gemoc Press, Sydney.

Watts, A.B., 2001. Isostasy and Flexure of the Lithosphere. Cambridge University Press.

Watts, A.B., Ryan, W.B.F., 1976. Flexure of the lithosphere and continental margin basins. Tectonophysics 36, 25–44.

Watts, A.B., Talwani, M., 1974. Gravity anomalies seaward of deep–sea trenches and their tectonic implications. Geophys. J. R. Astron. Soc. 36, 57–90.

Weissel, J.K., Anderson, R.N., Geller, C.A., 1980. Deformation of the Indo-Australian plate. Nature 287, 284–291.

Woodroffe, C.D., 1988. Vertical movement of isolated oceanic islands at plate margins: evidence from emergent reefs in Tonga (Pacific Ocean), Cayman Islands (Caribbean Sea) and Christmas Island (Indian Ocean). Z. Geomorphol., Suppl. 69, 17–37.

Yang, T., Moresi, L., Müller, R.D., Gurnis, M., 2017. Oceanic residual topography agrees with mantle flow predictions at long wavelengths. Geophys. Res. Lett. 44, 10,896–810,906.

Zhong, S., Gurnis, M., 1994. Controls on trench topography from dynamic models of subducted slabs. J. Geophys. Res. 99, 15,683–615,695.